ADVANCED FUNCTIONAL MATERIALS
www.afm-journal.de

Bioinspired Strong and Highly Porous Glass Scaffolds

Qiang Fu, Eduardo Saiz, and Antoni P. Tomsia*

The quest for more efficient energy-related technologies is driving the development of porous and high-performance structural materials with exceptional mechanical strength. Natural materials achieve their strength through complex hierarchical designs and anisotropic structures that are extremely difficult to replicate synthetically. We emulate nature's design by direct-ink-write assembling of glass scaffolds with a periodic pattern, and controlled sintering of the filaments into anisotropic constructs similar to biological materials. The final product is a porous glass scaffold with a compressive strength (136 MPa) comparable to that of cortical bone and a porosity (60%) comparable to that of trabecular bone. The strength of this porous glass scaffold is ~100 times that of polymer scaffolds and 4–5 times that of ceramic and glass scaffolds with comparable porosities reported elsewhere. The ability to create both porous and strong structures opens a new avenue for fabricating scaffolds for a broad array of applications, including tissue engineering, filtration, lightweight composites, and catalyst support.

1. Introduction

Natural materials are renowned for their unique combination of outstanding mechanical properties and exquisite microstructure. Trabecular (or cancellous) bone, cork, and wood are biological porous materials with high specific stiffness (stiffness per unit weight) and specific strength.[1–4] The outstanding mechanical properties of these natural materials are attributed to their anisotropic structures which are highly efficient in optimizing the strength-to-density and stiffness-to-density ratio.[1–5]

In materials science, the ability to develop porous constructs with high mechanical strength is important for a broad range of emerging applications, including filters,[4–7] catalyst supports,[8] and tissue engineering scaffolds.[9–11] Particularly for orthopedic surgery, the regeneration of large bone defects in load-bearing limbs remains a challenging problem. The compressive strength of cortical bone, primarily in the shaft of long bones and as the outer shell around trabecular bone, has been reported to be in the range of 100–150 MPa in the direction parallel to the axis of orientation (long axis).[12,13] It is difficult to design and fabricate a construct that will combine the large pores necessary to promote bone regeneration while substituting for, at least temporarily, the tissue by maintaining these loads in vivo. Porous metallic implants used for replacement in fractures have well-documented fixation problems,[14] and unlike natural bone, cannot self-repair or adapt to changing physiological conditions.[15] As a consequence, the implant becomes loose over time.[16] On the other hand, bioactive glass and ceramics have shown excellent potential in repair and regeneration of bone defects because of their widely recognized ability to support the growth of bone cells, strong bonding to hard and soft tissues, and adjustable degradation rate while newly formed bone and tissue are being remodeled.[9,17–19] The release of ions from bioactive glasses is also reported to activate the expression of osteogenic genes and to stimulate angiogenesis.[20–22] Recently, there has been increasing interest in using bioactive glass as a scaffold material for bone repair.[9,23–26] A variety of techniques have been used for the fabrication of glass scaffolds, including polymer foam replication,[23,24] sol-gel,[25] and freeze-casting.[26] However, the low compressive strength of these scaffolds (0.2–28 MPa for porosity of 92–60%) limits their application in the repair of load-bearing bone defects.

Here, we report the fabrication of bioactive glass scaffolds by direct-ink-write assembly of a hydrogel-based ink. Concentrated micrometer-sized ceramic inks are developed for robotic deposition of structures with characteristic feature sizes as fine as 30 μm. Porous glass scaffolds with combined high compressive strength (136 MPa) and porosity (60%) are obtained. The high mechanical strength combined with excellent in vitro bioactivity, demonstrated by the formation of nanometer-sized hydroxyapatite (HA) after immersion in simulated body fluid (SBF) for two weeks, indicates the great potential application of bioactive glass scaffolds in the repair and regeneration of load-bearing bone defects.

Direct ink writing as a layer-by-layer assembly technique has been used to fabricate constructs with materials including polymeric,[27] sol-gel,[28] and ceramic inks.[29,30] The technique can be used to build scaffolds whose structure follows a computer design. In that way, the scaffold architecture can be controlled and optimized to achieve the desired mechanical response, accelerate the bone regeneration process, and guide the formation of bone with the anatomic cortical-trabecular structure.[11] However, to achieve this goal, it will be necessary to design a process capable of printing a wide range of materials with

Dr. Q. Fu, Dr. A. P. Tomsia
Materials Sciences Division
Lawrence Berkeley National Laboratory
Berkeley, CA 94720, USA
E-mail: qfu@lbl.gov
Prof. E. Saiz
Centre for Advanced Structural Ceramics
Department of Materials
Imperial College London, London, UK

DOI: 10.1002/adfm.201002030

custom-made compositions and increased precision. In this respect, the formulation of concentrated inks with optimal rheological properties is crucial, as the ink has to be extruded through a fine nozzle in filamentary form and deposited over gaps that could be as large as 1–2 mm over the prior layer while maintaining the weight of the printed structure. Concentrated ceramic inks were formulated by dispersing ceramic particles in water and using polyethyleneimine (PEI) as a coagulant agent. The viscoelastic behavior of the ink was achieved by the interaction between the ammonium polyacrylate-based dispersant adsorbedon the particle surface and the ionized PEI.[31–33] However, a precise control of the amount of dispersant and PEI as well as careful manipulation of the pH is required, which is difficult with PEI-formulated inks. To design a flexible ink formulation that can print a wide range of ceramics, a hydrogel-based ink was developed by dispersing ceramic particles in a water-based solution of Pluronic F-127.[29] The ink showed good flowability and could be used to print various calcium-phosphate constructs, reaching a minimum line diameter of 100 μm. This approach is modified in the present study to prepare glass ink that can be easily printed into three dimensional scaffolds with increased precision. The glass selected is the bioactive 6P53B composition (in mol%: 51.9 SiO_2, 9.8 Na_2O, 1.8 K_2O, 15.0 MgO, 19.0 CaO, 2.5 P_2O_5), a composition specially designed for the improved coating of Ti and to expand the sintering window without crystallizing the glass.[34,35] Furthermore, this bioactive glass has shown significant advantages in promoting the osteointegration of Ti and for the fabrication of polymer/glass composites because of its relatively better stability in aqueous environments.[34–36] The good thermal behavior (glass transition temperature, T_g = 530 °C, softening point, T_s = 610 °C, and crystallization temperature, T_{cr} = 720 °C) and the ability to support cell growth warrant further study of 6P53B glass as a scaffold material for bone tissue engineering.

2. Results and Discussion

Glass particles with irregular shape (**Figure 1**a) and average diameter (D_{50}) of 1.2 μm (Figure 1b) were used to prepare the inks. The relatively wide particle size-distribution resulting from milling the glass powders contributes to a controlled flow of concentrated inks through narrow nozzles.[29] Glass ink consisted of 30 vol% 6P53B glass particles in aqueous solution with 20 wt% Pluronic F-127. The ink was loaded into a syringe, and then kept in an ice bath at 0 °C for 30 min to lower its viscosity. This cooling process was a key step for printing the glass ink through fine nozzles (down to 30 μm capillary tip, Figure 1), as Pluronic F-127 is a reverse thermoresponsive polymer and is capable of producing low viscosity aqueous solutions at lower temperatures, while forming a gel at higher temperatures.[37] The cooled glass ink was then extruded through a nozzle and printed inside an oil bath at 60 °C, which quickly induced the phase transition, or gelation, of Pluronic from an aqueous solution with relatively low viscosity to a gel. Typically, when using micrometer-sized particles, the forces required to extrude the gel-like inks through narrow tips (<100 μm) cause water segregation and clogging of the nozzles. Our approach allowed the printing of low-viscosity inks containing micrometer sized ceramic particles through capillaries as fine as 30 μm (Figure 1c,d).

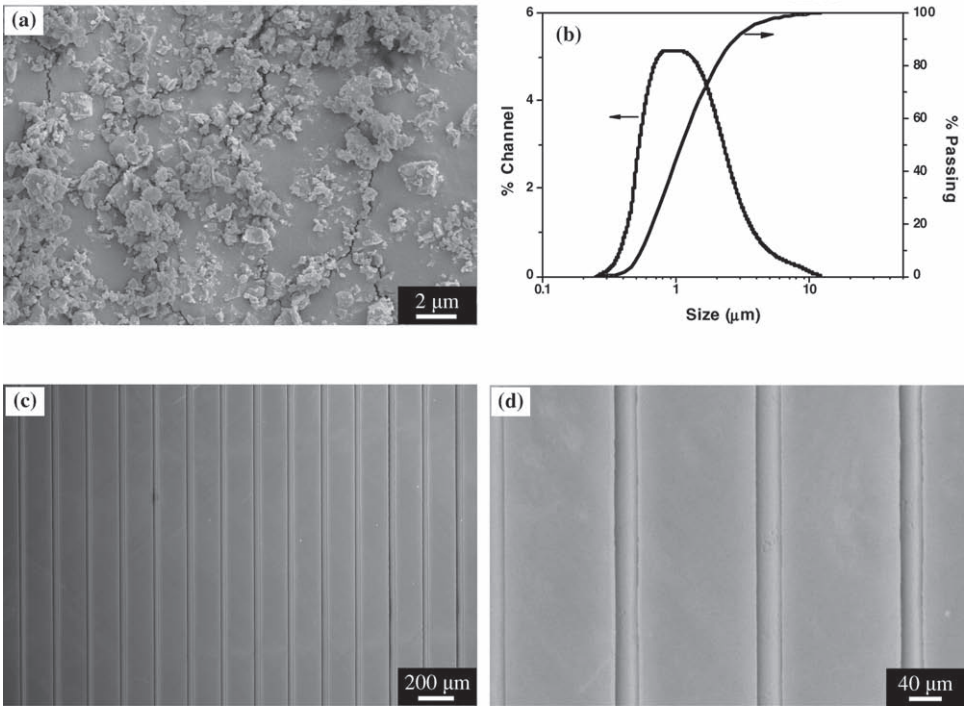

Figure 1. 6P53B glass particles used in the present work: a) SEM images of glass particles after attrition milling; b) the particle size distribution; patterns printed through 30 μm capillary tip using the hydrogel-based glass ink; c) as-printed parallel filaments; and d) high-magnification image of the filaments.

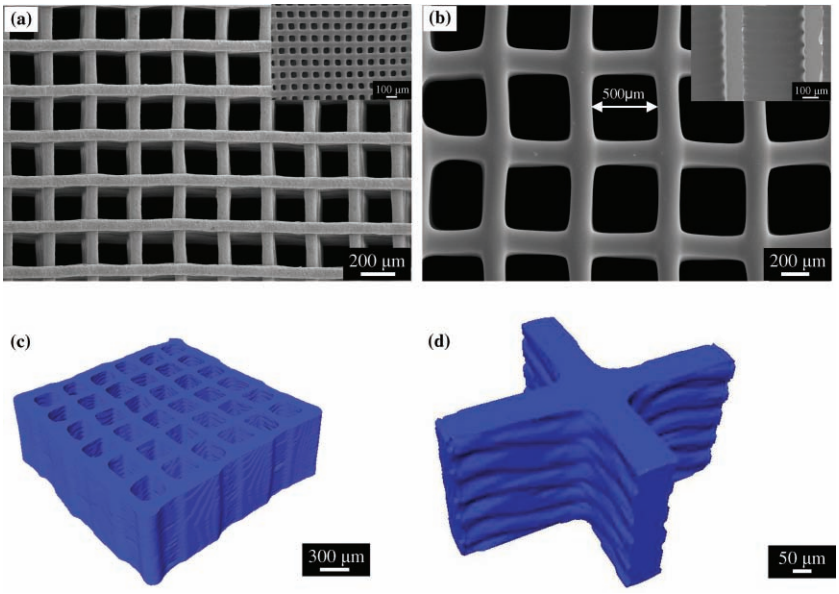

Figure 2. SEM images of (a) surface of as-printed 6P53B glass scaffolds through a 100 µm nozzle with a spacing of 200 µm, inset showing the scaffold after sintering; b) surface of sintered scaffolds with pores of 500 µm, inset showing cross section of the sintered scaffold; three-dimensional visualization of the sintered 6P53B glass scaffolds using synchrotron X-ray micro computed tomography. Images of (c) sintered scaffolds with regular grids; d) a sectional view of the bonded glass filaments.

Furthermore, the quick gelation of the ink upon contact with the heated oil prevented the fine features from collapsing and maintained their three-dimensional structures. Previous work has shown that 30 µm filaments can only be printed using inks containing $BaTiO_3$ nanoparticles.[38] Here, the possibility of achieving the same fine-featured structure with micrometer-sized glass particles dispersed in a hydrogel-based ink is realized by simply controlling the temperature of the ink.

To fabricate materials with high mechanical strengths, three-dimensional glass scaffolds with precisely defined filament diameter, spacing, and number of layers were patterned by extruding the glass ink through the 100 µm nozzles (**Figure 2**). Figure 2a shows the as-printed scaffold having a pore size of 200 µm with 72 layers. The softening point of the glass, T_s, is ~610 °C,[39] and the scaffolds were subjected to a binder burnout process at 600 °C for 2 h and then were sintered at 700 °C for 1 h to densify the glass filament while avoiding crystallization or deformation of the structure. After sintering, the glass scaffold consisted of struts with diameters of 100 µm and pores of 100 µm, as shown in the Figure 2a inset. Instead of rectangular pores in the as-printed scaffolds (Figure 2a), pores with round corners were observed as a result of the viscous-flow sintering of the glass. The sintering of the glass also led to the full densification of the glass rods with almost no closed porosity (Figure 2b inset), which resulted in increased mechanical strength.[24] For bone tissue engineering, scaffolds with high porosity and larger pore size are required to facilitate the ingrowth of hard and soft tissues. To increase the overall porosity and pore size, glass scaffolds with filament spans up to 500 µm were also fabricated (Figure 2b). Three-dimensional visualization of the sintered glass scaffolds was characterized by synchrotron X-ray micro computerized tomography (SR microCT). The scaffolds had a uniform structure with well bonded layers, as shown in Figure 2. Details of the layer fusion are shown in a cut-away section in Figure 2d. The constructs retained their shape with no noticeable deformation of the total structure (Figure 2c) after sintering. There was no closed porosity present within the sintered strut (Figure 2d), which was in good agreement with the SEM images shown in Figure 2b inset.

To determine the feasibility of using these scaffolds for the repair of load-bearing bone defects, their compressive strength in directions parallel and perpendicular to the pore channels was tested. Scaffolds with a dimension of 3 mm × 3 mm × 3 mm were used for the mechanical testing to determine the influence of pore orientation on mechanical performance. Samples were cut from the center of a 5 mm cube and subjected to surface grinding to eliminate the edge-effects and obtain parallel testing surfaces. To minimize errors associated with the use of small samples, particular care was taken in maintaining plane and parallel surfaces. These sample sizes are comparable to the scaffolds used for in vivo testing in small and medium animals while avoiding excessive machining, allowing an accurate recording of the load to failure. The compressive strength parallel to the pore channels was ~2.5 times of that measured in the perpendicular direction (136 ± 22 MPa vs. 55 ± 15 MPa), a reflection of the anisotropic structure of the scaffolds (Figure 2b and d).

The stress–strain curve, as shown in **Figure 3**a, indicated that the strength parallel to the pore orientation was as high as

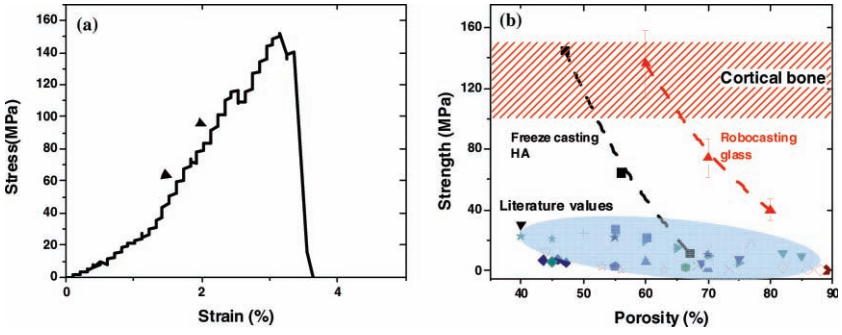

Figure 3. a) Stress–strain response of 6P53B glass scaffold under compression along the pore orientation (black triangles indicate the bumps in the curve); b) compressive strength vs. porosity of the scaffolds. Comparison with cortical bone[12,13] and literature values,[23–26,40–46] of porous glass and hydroxyapatite scaffolds. Each style of point corresponds to a different literature value; ▲ represents the data obtained in the present work on direct-ink-write assembly of 6P53B glass; ■ represents data obtained from freeze-casting of HA scaffolds.[46]

155 MPa for a typical glass scaffold with porosity of 60% and pore width of 500 μm (Figure 2b). The bumps in the stress–strain curve were due to the fracture of the walls upon compression, which is commonly observed in porous materials.[2] The elastic modulus, determined from the approximately linear region in the stress–strain curve, was 2.0 GPa, within the range of the value for trabecular bone (0.1–5 GPa).[12,13] The average strength (136 ± 22 MPa) is within the range of human cortical bone (100–150 MPa).[12,13] This value is 4–5 times the strength obtained for the bioactive glass and hydroxyapatite scaffolds with comparable porosity prepared by other conventional techniques,[23–26,40–46] as shown in Figure 3b. The strength is also at least two orders of magnitude higher than that of the polymeric scaffolds.[47] Figure 3b summarizes and compares the compressive strength of bioactive glass and ceramic scaffolds fabricated using different techniques. The summary is not meant to be exhaustive, but rather to indicate representative approaches. A detailed and comprehensive review of the mechanical behavior of calcium phosphate, CaP, composites is reported elsewhere.[48]

The curve of the compressive strength versus porosity of the glass scaffold shows a similar trend with that of the freeze-cast HA scaffolds, which consists of unidirectional pores. The high mechanical strength of the freeze-cast scaffold is attributed to its anisotropic structure consisting of parallel ceramic lamellae.[49,50] Anisotropic structure has been commonly observed in biological systems like wood, bone, cork, and glass sponge, and has been reported to be responsible for their ability to optimize efficiently the strength-to-density and stiffness-to-density ratio.[2,3,51] The work in this study might provide a new avenue for the fabrication of light, yet strong materials.

At porosities up to 60 vol%, the strength of glass scaffolds (136 MPa) is significantly higher than that of the freeze-cast HA scaffolds (Figure 3b). This might be due to the periodic structure consisting of parallel channels and the complete densification of the glass rods. In the glass scaffolds, dense solid walls were obtained after sintering, resulting in the oriented pore structure. As a result of their improved mass transport along pore orientation, scaffolds with oriented pores are reported to have better ability to support in vitro osteoblastic cell growth and neotissue formation than those with the same porosity but a random three-dimensional pore architecture.[52] The oriented pores also serve as guiding patterns for the directional migration of cells and tissues, and improve the in vitro and in vivo performance of scaffolds for axonal and nerve regeneration.[53–55] In addition, anisotropic materials are more likely to provide the required strength for load bearing applications in desired directions. For the glass scaffolds in this work, porosity in the direction perpendicular to the pore orientation can be introduced by lowering the sintering temperature or printing scaffolds through nozzles with a larger diameter (250 μm).

The mechanical behavior of cellular solids with close-cells has been well described by the Gibson and Ashby model.[2] According to the model, the compressive strength σ^*_{cr} of brittle cellular foams (ceramic or glass) is given by

$$\frac{\sigma^*_{cr}}{\sigma_{fs}} = 0.2\left(\phi\frac{\rho^*}{\rho_s}\right)^{3/2} + (1-\phi)\left(\frac{\rho^*}{\rho_s}\right) = 0.2\phi^{3/2}(1-P)^{3/2} + (1-\phi)(1-P) \quad (1)$$

where σ_{fs} is the modulus of rupture of the struts of the foam, Φ is the fraction of solid in the cell edge, ρ^* and ρ_s are the densities of the foam and the fully dense solid, respectively, and P is the porosity of the foam. In the case of the glass scaffold, the modulus of rupture of the strut was estimated as the tensile strength of the glass fiber with the similar diameter. The tensile strength of the glass fiber with the similar composition is reported to be 440 ± 151 MPa for a diameter of 93–160 μm.[56] As the solid is only present in the scaffold faces, Φ is 0. Based on these assumptions, the compressive strength of the glass scaffold was calculated to be 176 ± 60.4, 132 ± 45.3, and 88 ± 3 0.2 MPa for the porosities of 60, 70, and 80%, with the pore sizes of 500, 750, and 1000 μm, respectively. These calculated values are of the same magnitude as the measured compressive strength (136 ± 22, 74 ± 13, and 40 ± 7 MPa, respectively).

The X-ray diffraction spectra in **Figure 4** indicate that there was no crystalline phase formed in the glass scaffolds after sintering and the scaffold remained as an amorphous construct. Athough the presence of crystalline phases may result in higher strength, they can impair, at least partially, the bioactivity of glass scaffolds.[23] To further determine the suitability of glass scaffolds for the application of bone repair, their bioactivity was tested by immersion in SBF. After two weeks, the scaffold surface was covered with a layer of nanosized crystals (Figure 4a), which was confirmed to be HA by X-ray diffraction (Figure 4b). Further analysis (not shown here) using Fourier transform infrared spectroscopy (FTIR) also indicated formation of a carbonate-substituted HA layer on the surface, which corresponded well with our previous work on the glass.[35] The thickness of the layer was determined to be ~5 μm by observing the cross sections using SEM (Figure 4a). The formation of the HA on the glass surface has been reported to be responsible for the strong bonding between the scaffold and hard tissues.[9,19] The fast formation of the nanosized HA layer is usually considered an indication of good in vitro bioactivity. Our processing approach does not crystallize or degrade the bioactive behavior of the 6P53B glass.

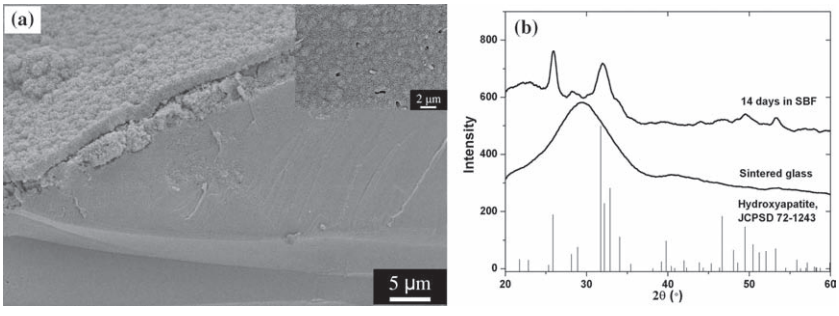

Figure 4. Surface reaction layer of 6P53B glass scaffold after immersion in simulated body fluid (SBF) for two weeks. (a) SEM images showing the glass filament covered with fine nanosized hydroxyapatite crystals (inset showing detailed morphology of the crystals); (b) X-ray diffraction pattern of the formed crystals.

3. Conclusions

In conclusion, we have developed highly porous and strong glass scaffolds by direct-ink-write assembly of a hydrogel-based glass ink. The technique enables precise manipulation of the three-dimensional structure and printing of lines as thin as 30 μm using micrometer-sized ceramic powders. The sintered glass scaffolds with anisotropic structure show a compressive strength comparable to human cortical bone, an indication of their excellent potential for the repair and regeneration of load-bearing bone defects. The ability to create both porous and strong structures opens a new avenue for fabricating scaffolds for a broad array of applications, including tissue engineering, filtration, lightweight composites, and catalyst support. In the field of bone regeneration, the use of glasses also opens new possibilities, as their composition can be easily tailored to manipulate bioactivity and biodegradation rates as well as the release kinetics of different ions.

4. Experimental Section

Materials: Bioactive 6P53B glass with the composition (mol%): 51.9 SiO_2, 9.8 Na_2O, 1.8 K_2O, 15.0 MgO, 19.0 CaO, 2.5 P_2O_5, was purchased from SEM-COM (SEM-COM Company, Toledo, OH). Particles of D_{50} = 1.2 μm were obtained by sieving the glass to a size <75 μm, followed by wet attrition milling (Model 01-HD, Union Process, Akron, OH). The inks were created by mixing 30 vol% glass particles in 20 wt% Pluronic F-127 solution. After dispersing the glass particles, commercial corn syrup (Karo) (4 wt% solution in water) was added to enhance adhesion between printed filaments. To homogenize the ink, it was placed in a refrigerator at 4 °C overnight. Before printing, the ink was sieved through a 25 μm mesh to minimize the presence of aggregates. The ink was loaded into a 10 mL syringe (BD, Franklin Lakes, NJ) with an HD-PTFE custom-sized plunger.

Direct-Write Assembly of Glass Scaffolds: Glass scaffolds were fabricated by printing the inks through a 100 μm nozzle (EFD precision tips, EFD, East Providence, RI) using a robotic deposition device (RoboCAD 3.0, 3-D Inks, Stillwater, OK). Glass ink was first loaded into a syringe and then kept in an ice bath for 30 min to cool the ink to lower the viscosity. The inks were printed on an Al_2O_3 substrate (3 mm thick) inside a reservoir of nonwetting oil (Lamplight, Menomonee Falls, WI) heated at 60 °C. The Al_2O_3 substrate was coated with an oil-soluble hydrophobic layer (Sharpie permanent marker, Newell Rubermaid, Atlanta, GA) before printing. The printed scaffolds were easily detached from the substrate after the oil dissolved the hydrophobic layer.

After printing, the scaffolds were air-dried for 24 hours and subjected to a controlled-heat treatment to decompose the organics and sinter the glass particle into dense filaments. The green samples were heated at 1 °C/min to 600 °C in flowing O_2 gas, and then at 5 °C/min to 700 °C, and kept for 1 h.

Characterization: The porosity of the sintered glass scaffolds was measured using the Archimedes method. Scanning electron microscopy, SEM, (Hitachi S-4300, Tokyo, Japan) was used to observe the microstructure of the scaffolds. The samples were sputter-coated with Au and examined at an accelerating voltage of 10 kV.

X-ray diffraction (XRD) (Siemens D500, Munich, Germany) was used to identify the phases present in the starting powder and sintered samples, using Cu Ka radiation (λ = 0.15406 nm) at a scanning rate of 1.8°/min in the 2θ range of 20–80°.

Synchrotron X-ray micro computerized tomography was used to obtain a three-dimensional perspective of the scaffold. Scanning was conducted at the Advanced Light Source (ALS-LBNL, Berkeley, CA) with 22 keV monochromatic X-rays and a 4.4 μm voxel size (resolution). The data sets were reconstructed using Octopus software and the three-dimensional visualization was performed using Avizo software.

The compressive strength of the glass scaffolds was measured by performing uniaxial tests on cubic blocks (3 mm × 3 mm × 3 mm) cut from the sintered specimens using a low speed saw. Surface grinding was conducted on the blocks to ensure that the two tested ends were flat and parallel. The samples were compressed in the direction parallel to the pore orientation on a servo-hydraulic testing machine (MTS810, MTS Systems, Eden Prairie, MN) at a cross-head speed of 0.5 mm/min. At least eight samples were tested to get statically reliable values.

Acknowledgements

This work was supported by the National Institutes of Health/National Institute of Dental and Craniofacial Research (NIH/NIDCR) Grant No. 1 R01 DE015633. We acknowledge support of the dedicated X-ray tomography beamline 8.3.2 at the Advanced Light Source (ALS), funded by Department of Energy under Contract No. DE-AC02–05CH11231. ES is grateful for the support from EPRSC.

Received: September 26, 2010
Revised: November 18, 2010
Published online: February 7, 2011

[1] M. F. Ashby, L. J. Gibson, U. Wegst, R. Olive, *Proc. R. Soc. Lond. A* **1995**, *450*, 141.
[2] L. J. Gibson, M. F. Ashby, *Cellular Solids, Structure and Properties*, Cambridge Univ. Press, Cambridge **1999**.
[3] P. Fratzl, R. Weinkamer, *Prog. Mater. Sci.* **2007**, *52*, 1263.
[4] J. Keckes, I. Burgert, K. Frühmann, M. Müller, K. Kölln, M. Hamilton, M. Burghammer, S. Roth, S. Stanzl-Tschegg, P. Fratzl, *Nat. Mater.* **2003**, *2*, 810.
[5] J. D. Curry, *J. Exp. Biol.* **1999**, *202*, 3285.
[6] P. Colombo, *Science* **2008**, *322*, 381.
[7] A. J. Pyzik, C. G. Li, *Inter. J. Appl. Ceram. Tech.* **2005**, *2*, 440.
[8] M. V. Twigg, J. T. Richardson, *Ind. Eng. Chem. Res.* **2007**, *46*, 4166.
[9] L. L. Hench, J. M. Polak, *Science* **2002**, *295*, 1014.
[10] R. Langer, J. P. Vacnti, *Science* **1993**, *260*, 920.
[11] S. J. Hollister, *Nat. Mater.* **2005**, *4*, 518.
[12] J. Y. Rho, M. C. Hobatho, R. B. Ashman, *Med. Eng. Phys.* **1995**, *17*, 347.
[13] Y. C. Fung, *Biomechanics: mechanical properties of living tissues*, Springer, New York **1993**.
[14] *R&D Priorities for Biomaterials and Implants*. UK Department of Health, London **1996**.
[15] H. R. Piehler, *MRS Bull.* **2000**, *25*, 67.
[16] R. Huiskes, H. Weinans, B. Vanrietbergen, *Clin. Orth. Rel. Res.* **1992**, *274*, 124.
[17] L. L. Hench, J. Wilson, *Science* **1984**, *226*, 630.
[18] D. L. Wheeler, K. E. Stokes, H. M. Park, J. O. Hollinger, *J. Biomed. Mater. Res.* **1997**, *35*, 249.
[19] L. L. Hench, *J. Am. Ceram. Soc.* **1998**, *81*, 1705.
[20] I. D. Xynos, A. J. Edgar, L. D. Buttery, L. L. Hench, J. M. Polak, *J. Biomed. Mater. Res. Appl Biomater* **2001**, *55*, 151.
[21] K. J. Leach, D. Kaigler, Z. Wang, P. H. Krebsbach, D. J. Mooney, *Biomaterials* **2006**, *27*, 3249.
[22] A. Leu, J. K. Leach, *Pharm. Res.* **2008**, *25*, 1222.
[23] Q. Z. Chen, A. Efthymiou, V. Salih, A. R. Boccaccini, *Biomaterials* **2006**, *27*, 2414
[24] Q. Fu, M. N. Rahaman, B. S. Bal, D. E. Day, *Acta Biomater.* **2008**, *4*, 1854.
[25] J. R. Jones, L. M. Ehrenfried, L. L. Hench, *Biomaterials* **2006**, *27*, 964.
[26] Q. Fu, M. N. Rahaman, B. S. Bal, R. F. Brown, *J. Biomed. Mater. Res.* **2010**, *93A*, 1380.

[27] G. M. Gratson, M. Xu, J. A. Lewis, *Nature* **2004**, *428*, 386.
[28] B. Y. Ahn, E. B. Duoss, M. J. Motala, X. Guo, S. Park, Y. Xiong, J. Yoon, R. G. Nuzzo, J. A. Rogers, J. A. Lewis, *Science* **2009**, *323*, 1590.
[29] J. Franco, P. Hunger, M. E. Launey, A. P. Tomsia, E. Saiz, *Acta Biomater.* **2010**, *6*, 218.
[30] J. A. Lewis, J. E. Smay, J. Stuecker, J. Cesarano III, *J. Am. Ceram. Soc.* **2006**, *89*, 3599.
[31] S. Michna, W. Wu, J. A. Lewis, *Biomaterials* **2005**, *26*, 5632.
[32] P. Miranda, E. Saiz, K. Gryn, A. P. Tomsia, *Acta Biomater.* **2006**, *2*, 457.
[33] J. E. Smay, G. M. Gratson, R. F. Shepherd, J. Cesarano, J. A. Lewis, *Adv. Mater.* **2002**, *14*, 1279.
[34] A. Pazo, E. Saiz, A. P. Tomsia, *Acta Mater.* **1998**, *46*, 2551.
[35] S. Lopez-Esteban, C. F. Gutierrez-Bonzalez, L. Gremillard, E. Saiz, A. P. Tomsia, *J. Biomed. Mater. Res.* **2009**, *88A*, 1010.
[36] J. Russias, E. Saiz, S. Deville, K. Gryn, G. Liu, R. K. Nalla, A. P. Tomsia, *J. Biomed. Mater. Res.* **2007**, *83A*, 434.
[37] D. Cohn, A. Sosnik, S. Garty, *Biomacromolecules* **2005**, *6*, 1168.
[38] Q. Li, J. A. Lewis, *Adv Mater.* **2003**, *15*, 1639.
[39] S. Lopez-Esteban, E. Saiz, S. Fujino, T. Oku, K. Suganuma, A. P. Tomsia, *J. Eur. Ceram. Soc.* **2003**, *23*, 2921.
[40] C. V. Brovarone, E. Verné, P. Appendino, *J. Mater. Sci Mater. Med* **2006**, *17*, 1069.
[41] Q. Fu, M. N. Rahaman, B. S. Bal, W. H. Huang, D. E. Day, *J. Biomed. Mater. Res.* **2007**, *82A*, 222.
[42] Q. Z. Chen, A. Efthymiou, V. Salih, A. R. Boccaccini, *J. Biomed. Mater. Res.* **2008**, *84A*, 1049.
[43] H. Zhang, X. J. He, J. S. Li, *Biomed. Mater.* **2009**, *4*, 045007.
[44] S. C. Wu, H. C. Hus, S. H. Hsiao, W. F. Ho, *J. Mater. Sci. Mater. Med* **2009**, *20*, 1229.
[45] H. Fu, Q. Fu, N. Zhou, W. H. Huang, M. N. Rahaman, D. P. Wang, X. Liu, *Mater. Sci. Eng. C* **2009**, *29*, 2275.
[46] S. Dveille, E. Saiz, A. P. Tomsia, *Biomaterials* **2006**, 5480.
[47] K. Rezwan, Q. Z. Chen, J. J. Blaker, A. R. Boccaccini, *Biomaterials* **2006**, *27*, 3413.
[48] A. J. Wagoner Johnson, B. A. Herschler, *Acta Biomater.* **2011**, *7*, 16.
[49] S. Deville, E. Saiz, R. K. Nalla, A. P. Tomsia, *Science* **2006**, *311*, 515.
[50] E. Munch, M. E. Launey, D. H. Alsem, E. Saiz, A. P. Tomsia, R. O. Ritchie, *Science* **2008**, *322*, 1516.
[51] M. A. Meyers, P. Chen, A. Y. Lin, Y. Seki, *Prog. Mater. Sci.* **2008**, *53*, 1.
[52] P.X. Ma, R. Zhang, *J. Biomed. Mater. Res.* **2001**, *56*, 469.
[53] S. Stokols, M. H. Tuszynski, *Biomaterials* **2004**, *25*, 5839.
[54] T. T. Yu, M. S. Shoichet, *Biomaterials* **2005**, *26*, 1507.
[55] J. Li, T. A. Rickett, R. Shi, *Langmuir* **2009**, *25*, 1813.
[56] E. Pirhonen, H. Niiranen, T. Niemelä, M. Brink, P. Tömälä, *J. Biomed. Mater. Res. B Appl. Biomater.* **2006**, *77B*, 227.